

Subsurface damage and bending strength analysis for ultra-thin and flexible silicon chips

JIAN Wei^{1,2}, WANG ZhaoXian^{3,4}, JIN Peng^{1,2}, ZHU LongJi^{1,2,3},
CHEN Ying^{3,4*} & FENG Xue^{1,2*}

¹ Key Laboratory of Applied Mechanics of Ministry of Education, Department of Engineering Mechanics, Tsinghua University, Beijing 100084, China;

² Center for Flexible Electronics Technology, Tsinghua University, Beijing 100084, China;

³ Institute of Flexible Electronics Technology of Tsinghua University Jiaxing, Jiaxing 314000, China;

⁴ Qiantang Science and Technology Innovation Center, Hangzhou 310016, China

Received November 30, 2021; accepted March 1, 2022; published online July 18, 2022

Subsurface damage (SSD) is an unavoidable problem in the precision mechanical grinding for preparing ultra-thin and flexible silicon chips. At present, there are relatively few studies on the relationship between SSD and the bending strength of ultra-thin chips under different grinding parameters. In this study, SSD including amorphization and dislocation is observed using a transmission electron microscope. Theoretical predictions of the SSD depth induced by different processing parameters are in good agreement with experimental data. The main reasons for SSD depth increase include the increase of grit size, the acceleration of feed rate, and the slowdown of wheel rotation speed. Three-point bending test is adopted to measure the bending strength of ultra-thin chips processed by different grinding conditions. The results show that increasing wheel rotation speed and decreasing grit size and feed rate will improve the bending strength of chips, due to the reduction of SSD depth. Wet etching and chemical mechanical polishing (CMP) are applied respectively to remove the SSD induced by grinding, and both contribute to providing a higher bending strength, but in comparison, CMP works better due to a smooth surface profile. This research aims to provide some guidance for optimizing the grinding process and fabricating ultra-thin chips with higher bending strength.

ultra-thin chip, flexible chip, subsurface damage, bending strength, mechanical grinding

Citation: Jian W, Wang Z X, Jin P, et al. Subsurface damage and bending strength analysis for ultra-thin and flexible silicon chips. *Sci China Tech Sci*, 2022, 65, <https://doi.org/10.1007/s11431-021-2021-4>

1 Introduction

Ultra-thin chips (with a thickness below 50 μm) exhibit high flexibility and significant deformability for low bending stiffness [1–3]. As the core of signal processing and transmission, ultra-thin and flexible chips play a key role in high-performance flexible electronics [4–6]. However, limited by the intrinsic material properties [7–9] (i.e., high hardness,

high brittleness, and low fracture toughness) of inorganic semiconductor materials, the fabrication of ultra-thin chips becomes a tricky challenge. Up to now, a wide range of technologies have been attempted to realize ultra-thin chips, including mechanical grinding [10], laser lift-off [11,12], dry etching [13], silicon on insulator (SOI) wafer-based transfer printing [14], and epitaxy based on porous silicon [15].

Among these thinning methods, mechanical grinding is widely used in the industry to thin integrated circuit (IC) wafers after front-end fabrication by removing the backside substrate. However, irreversible subsurface damage (SSD)

*Corresponding authors (email: chenying@ifet-tsinghua.org; fengxue@tsinghua.edu.cn)

including microcrack, phase transformation, and dislocation may occur in the material removal process [16–19]. The SSD leads to residue stress, wrappage, and even breakage of chips [20,21], which causes performance degradation and low yield of intact ultra-thin chips. To understand and diminish SSD, the grinding process has been investigated both experimentally and theoretically. Previous studies [22–26] have been conducted to investigate the relationship between the SSD and grinding parameters, considering the subsurface crack depth as the SSD depth based on the fracture mechanics theory. However, these studies are no longer applicable when dislocation-mediated plasticity is dominated and crack formation is suppressed in the high-quality grinding process of ultra-thin chips [27]. Furthermore, bending strength [28,29] is an important mechanical characteristic in terms of evaluating the failure resistance of the chip. Many scholars have attempted to study the effect of the grinding process on bending strength. For example, Jeon et al. [30] and McLellan et al. [31] proposed that the bending strength of chips was determined by surface roughness and morphology. Liu et al. [32] discussed the influence of surface crack inclination angle on bending strength. Wu et al. [33] and Yang et al. [34] revealed that bending strength depended on the distribution direction of surface scratches. Yang et al. [34] analyzed the relationship between residue stress and bending strength. These existing studies focus on exploring the way in which surface characterization affects the bending strength of ultra-thin chips without considering the SSD. In fact, interior material defects also severely impact chip performance, but there are relatively few studies investigating the effect of SSD on bending strength under different grinding conditions.

In this study, SSD including amorphization and dislocation is observed by transmission electron microscope (TEM). The SSD depths of chips under different processing parameters are predicted theoretically. Three-point bending tests are used to measure the bending strength of chips processed with different grinding parameters. The way in which SSD induced by the grinding process influences the bending strength of ultra-thin chips is also discussed. Hopefully, this work can bring some guiding light to the grinding process, for the further optimization of ultra-thin and flexible chips.

2 Materials and methods

2.1 Materials

Single crystal (100) silicon wafers grown by the Czochralski (CZ) method (Li Jing Photonics Co. Ltd., Quzhou, China) with high purity (undoped, resistance > 1000 Ω cm) are used in this study as starting materials. The initial wafer thickness is 750 μ m and the diameter is 150 mm.

2.2 Mechanical grinding

Mechanical grinding tests of single crystal Si wafer are conducted on a precision surface grinder (DAG 810, Disco, Japan). Resin-bond diamond wheels with respective grain sizes of #600, #3000, and #8000 are used in this study. The outer diameter of the grinding wheel is 203 mm, and the width of a wheel segment is 3 mm. The wheel rotation speed, feed rate, and wafer rotation speed are adjustable as needed. During the grinding process, deionized water is adopted to diffuse the heat generated by grinding.

2.3 Characterization

To remove contaminants that may be potentially adsorbed, each sample is ultrasonically cleaned in ethanol for approximately 3 min, washed with deionized water, and dried in pure nitrogen before the tests. The scanning electron microscope (SEM, Merlin, Zeiss, Germany) is used to observe the surface topography of the wafers after grinding. The morphology and roughness of the ground surface are examined by using an atomic force microscope (AFM, Bruker AXS, Bruker, USA). The focused ion beam technique (FIB, Auriga, Zeiss, Germany) is used to prepare the cross-sectional TEM specimens. The transmission electron microscope (TEM, Tecnai G2 F30, FEI, USA) is used to observe subsurface damage and deformation.

2.4 Three-point bending test

Ultra-thin chips with a plane size of 10 mm \times 5 mm are prepared from silicon wafers using a dicing saw (DFD 6240, Disco, Japan) after the grinding process. Three-point bending tests (Sigma lite, XYZTEC, Holland) are performed to evaluate the bending strength of the fabricated ultra-thin chips. The distance between two supports is set as 3 mm and the loading rate is 50 μ m/s. The whole test process is completed automatically, and the corresponding test data can be read freely.

3 Results and discussion

3.1 Theoretical prediction of subsurface damage (SSD) depth

The specific grinding process is illustrated in Figure 1(a). The unprocessed single crystal silicon wafer is held on a vacuum chuck, and the grinding wheel and wafer simultaneously rotate around their respective axes. At the same time, the grinding wheel feeds down towards the wafer. The material removal in the thinning process is actually attributed to the friction and wear between the abrasive grits and workpiece. When the diamond grits scratch the surface of the

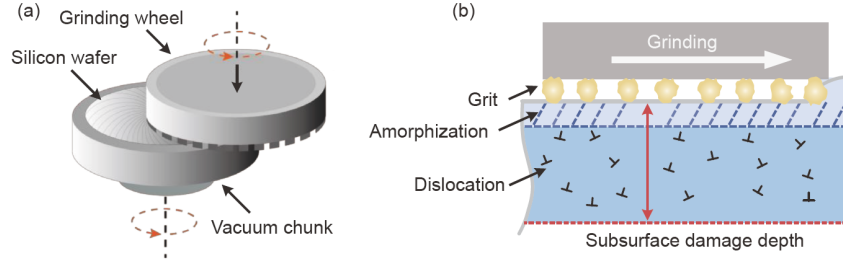


Figure 1 (a) Schematic illustration of the grinding process; (b) subsurface damage induced by the grinding process.

silicon wafer, irreversible subsurface damage including amorphization and dislocation is formed beneath the grits. Here, the maximum depth of dislocation extending downward from the surface is defined as the SSD depth, as shown in Figure 1(b).

In order to clarify the relationship between the process parameters and SSD, theoretical analysis is first conducted. Controlled by the process parameters, the normal grinding force between the abrasive grits and the wafer surface is a crucial factor leading to the SSD. For a single abrasive grit, the relationship between the normal grinding force P and the process parameters is given by [35]

$$P = \left(5.08E_r R_e^2 + 8.08kR_e^2 \right) \left(\frac{rfN_w}{\gamma L W N_s^2 (1 + r^2/8R_s^2)} \right)^{0.6}, \quad (1)$$

where R_e represents the average grit size, f represents the feed rate, and N_s represents the wheel rotation speed; E_r is the reduced Young's modulus, calculated from the elastic constants for the silicon wafer and diamond grit, $1/E_r = (1 - \nu_1^2)/E_1 + (1 - \nu_2^2)/E_2$; E_1 and ν_1 are the Young's modulus and Poisson ratio of the silicon wafer, respectively, and E_2 and ν_2 are the Young's modulus and Poisson ratio of the diamond grit, respectively; k is the material constant referred to as the chip thickness coefficient; L , W , γ , and R_s are the constant geometry parameters of the wheel; N_w is the wafer rotation speed; r is the radial distance from the center of the wafer. Detailed material properties [7–9] and experimental parameters are provided in the Supporting Information, Table S1.

In fact, dislocations, as one-dimensional defects in crystals, are the main carriers of plastic deformation that are generated during grinding. Based on the Mises yield criterion, the plastic zone size δ (i.e., the dislocation depth) induced in the scratching process is determined by [36]

$$\delta = \sqrt{\frac{P}{\pi H}} \left[\frac{3(1-2\nu_1)}{5-4\nu_1} + \frac{2\sqrt{3}}{\pi(5-4\nu_1)} \frac{E_1}{\sigma_y} \cot\alpha \right]^{0.5}, \quad (2)$$

where H represents the hardness of the silicon wafer, and σ_y represents the yield strength of silicon wafer; α is the grit geometry angle. Substituting eq. (1) into eq. (2), the relationship between the SSD depth and process parameter is

obtained, as shown below:

$$\delta = \psi \frac{f^{0.3} R_e}{N_s^{0.6}} (5.08E_r + 8.08k)^{0.5} \cdot \left[\frac{3(1-2\nu_1)}{\pi H(5-4\nu_1)} + \frac{2\sqrt{3}}{\pi^2(5-4\nu_1)} \frac{E_1}{H\sigma_y} \cot\alpha \right]^{0.5}, \quad (3)$$

where $\psi = (rN_w)^{0.3} (LW\gamma)^{-0.3} (1 + r^2/(8R_s^2))^{-0.3}$ is an invariant for a certain grinding process. From eq. (3), it can be seen that the grit size, rotation speed, and feed rate of the grinding wheel are the main parameters that determine machining quality. In particular, the SSD depth is proportional to the grit size and feed rate, and inversely proportional to the rotation speed. Besides, the grit size has a larger exponent than the other two parameters, which means that grid size should have a greater influence on the SSD depth.

3.2 Effects of process parameters on SSD depth

3.2.1 Grit size

In order to explore the SSD induced by different grit sizes, the silicon wafer is ground using three types of grinding wheels, with the same feed rate (0.1 $\mu\text{m/s}$) and wheel rotation speed (3000 r/min). The average grit sizes are approximately 23, 4.3, and 1.8 μm , respectively, corresponding to #600, #3000, and #8000 grinding wheels. The surface topography of the wafers observed by SEM and AFM is shown in the Supporting Information, Figure S1. As grit size decreases, the average surface roughness R_a decreases significantly. The induced SSD in the grinding process is further analyzed through TEM observations. The focused ion beam technique (FIB) is used to prepare the cross-sectional TEM specimens. No additional damage is introduced during the sample preparation, guaranteed by a protective layer of Pt that is coated on the ground surface. The cross-sectional image of the TEM sample is shown in Figure S2.

Figure 2(a) and (b) show representative TEM images of SSD after grinding with different grit sizes. The diffraction pattern taken from the top region (shown in the inset of Figure 2(a)) indicates the existence of an amorphous layer, which should be attributed to high levels of pressure between the diamond grit and the sample surface [37]. The diffraction

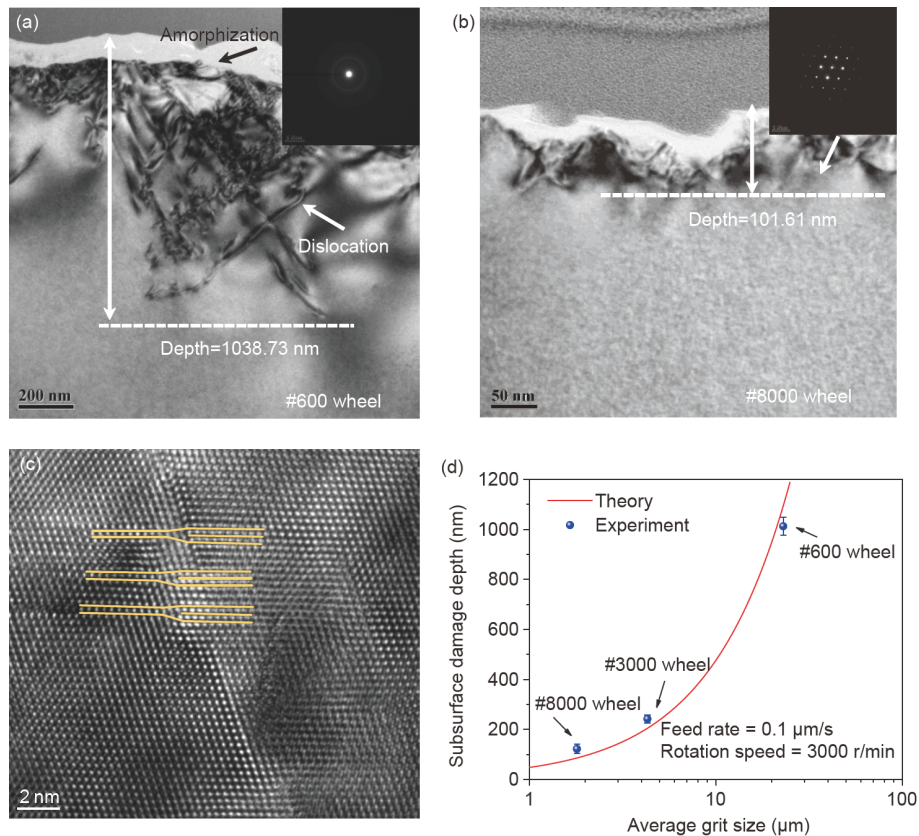


Figure 2 Representative TEM image showing SSD induced by (a) a #600 wheel, where the inset image shows the diffraction pattern of the amorphization region and (b) a #8000 wheel, where the inset image shows the diffraction pattern below the amorphization layer. (c) HR-TEM image of dislocations, yellow lines highlight the edge dislocation. (d) Variation of SSD depth with average grit size (the horizontal axis is provided in logarithmic coordinates).

pattern taken from the plastic region indicates the existence of a single crystal structure, as shown in the inset of Figure 2(b). When local shear stress reaches the critical shear strength, the plastic zone will be yielded, and the dislocation will occur. The TEM images show that a dislocation slip line is present just below the amorphous layer. The high resolution (HR)-TEM image of the region near the slip line in Figure 2(c) clearly indicates an extra half-plane of atoms, which is the typical feature of edge dislocations. For each grit size, the average SSD depth and relative error of the samples are measured in TEM images. According to eq. (3), in logarithmic coordinates on the horizontal axis, the relationship between SSD depth and average grit size is predicted theoretically, as shown in Figure 2(d). This theoretical prediction is in good agreement with the experimental data. As grit size decreases, the depth of SSD is also reduced. From eqs. (1) and (2), the main reason for the above results is a reduction of normal grinding force between the diamond grit and sample surface. Provided that other conditions are invariant, when the grit size decreases, the stress field of the grit-wafer interaction is weakened, which may be attributed to a lower normal grinding force. Decreasing grinding stress will induce less elastic-plastic deformation and lower SSD depth.

3.2.2 Wheel rotation speed

To clarify the effect of wheel rotation speed on the SSD depth, the ultra-thin chips are processed under different wheel rotation speeds with the same grit size (#3000 wheel) and feed rate (0.5 $\mu\text{m/s}$). The representative TEM images of the SSD for wheel rotation speeds of 2000 and 5000 r/min are shown in Figure 3(a) and (b). The theoretical SSD depth under different wheel rotation speeds is predicted by eq. (3), which is verified by the experimental results, as shown in Figure 3(c). These results show that SSD depth decreases with increasing wheel rotation speed. This can be explained by the fact that, with increasing wheel rotation speed, the depth-of-cut and the number of effective abrasive grains participating in the grinding decrease, resulting in a lower normal grinding force [35]. Therefore, the grinding stress beneath the abrasive grit decreases, which causes smaller elastic-plastic deformation and lower SSD depth.

3.2.3 Feed rate

The effect of feed rate is also investigated in a similar way. The ultra-thin chips are processed under different feed rates with the same grit size (#3000 wheel) and wheel rotation speed (3000 r/min). Figure 4(a) and (b) show typical TEM images of SSD with feed rates of 0.1 and 0.5 $\mu\text{m/s}$. The

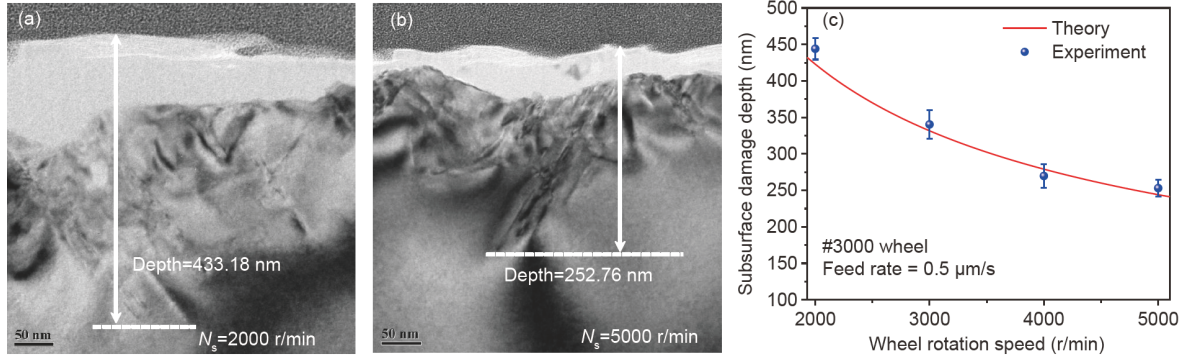


Figure 3 Representative TEM images showing SSD induced by wheel rotation speeds of (a) 2000 r/min and (b) 5000 r/min. (c) Variation of SSD depth with wheel rotation speed.

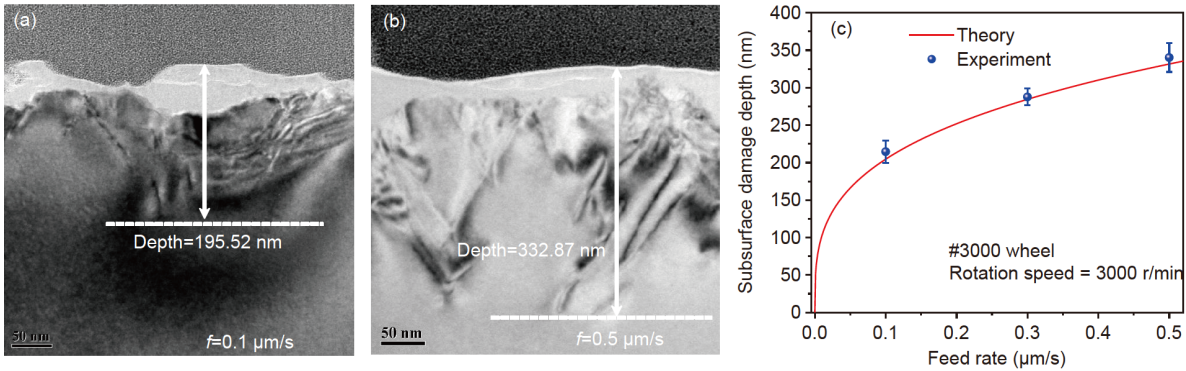


Figure 4 Representative TEM images showing SSD induced by feed rates of (a) 0.1 $\mu\text{m/s}$ and (b) 0.5 $\mu\text{m/s}$. (c) Variation of SSD depth with the feed rate.

experimental data (discrete points in Figure 4(c)) are in good agreement with the prediction eq. (3). The results reveal that the SSD depth increases with increasing feed rate. This is because more intense interactions and normal grinding force between the grit and chips occur as the feed rate increases. Hence, the grinding stress increases, which induces larger elastic-plastic deformation and deeper SSD depth.

3.3 Effects of process parameters on bending strength

Bending strength is an important mechanical character of ultra-thin and flexible chips. In order to study the bending strength variation under different process parameters, the ultra-thin chips with the plane-size of 10 mm \times 5 mm and thickness of 30 μm are prepared from silicon wafer after grinding. The three-point bending test is an effective method to measure the bending strength of ultra-thin chips. Figure 5(a) shows an image of the silicon chip during a bending test. The upper side of the chip is compressed, and the lower side is in tension. A typical load-displacement curve for the bending test is shown in Figure S3. The fracture force of each chip is recorded at the curve peak, and the bending strength for each silicon chip is determined as follows:

$$\sigma = \frac{3FL}{2bh^2}, \quad (4)$$

where F is the fracture force, L is the distance between the two supporting points, b is the width of the chip, and h is the thickness of the chip.

To understand the relationship between bending strength and grit size, the bending strength is measured for chips machined by different grit sizes with the same feed rate (0.1 $\mu\text{m/s}$) and wheel rotation speed (3000 r/min), as shown in Figure 5(b). The situations in which SSD is on the top or on the bottom are both considered. In the case that SSD is located on the tensile side (i.e., SSD on the bottom), the average bending strengths are 122, 373, and 568 MPa for #600 wheel, #3000 wheel and #8000 wheel, respectively. However, when SSD is located on the compressed side (i.e., SSD on the top), the average bending strengths are improved to 335, 462, and 607 MPa, respectively. In this case, the crack initiation and propagation are suppressed under the compressive stress, thereby indirectly increasing the bending strength. Besides, it is evident that the bending strength becomes higher with decreasing grit size, which agrees with the variation of SSD depth with the average grit size shown in Figure 2(d). Instructed by the above result, arranging the damage layer on the compressed side may enable the higher flexural performance of devices in practical applications.

To explore the effect of wheel rotation speed, the bending strength is measured for ultra-thin chips processed under different wheel rotation speeds with the same grit size

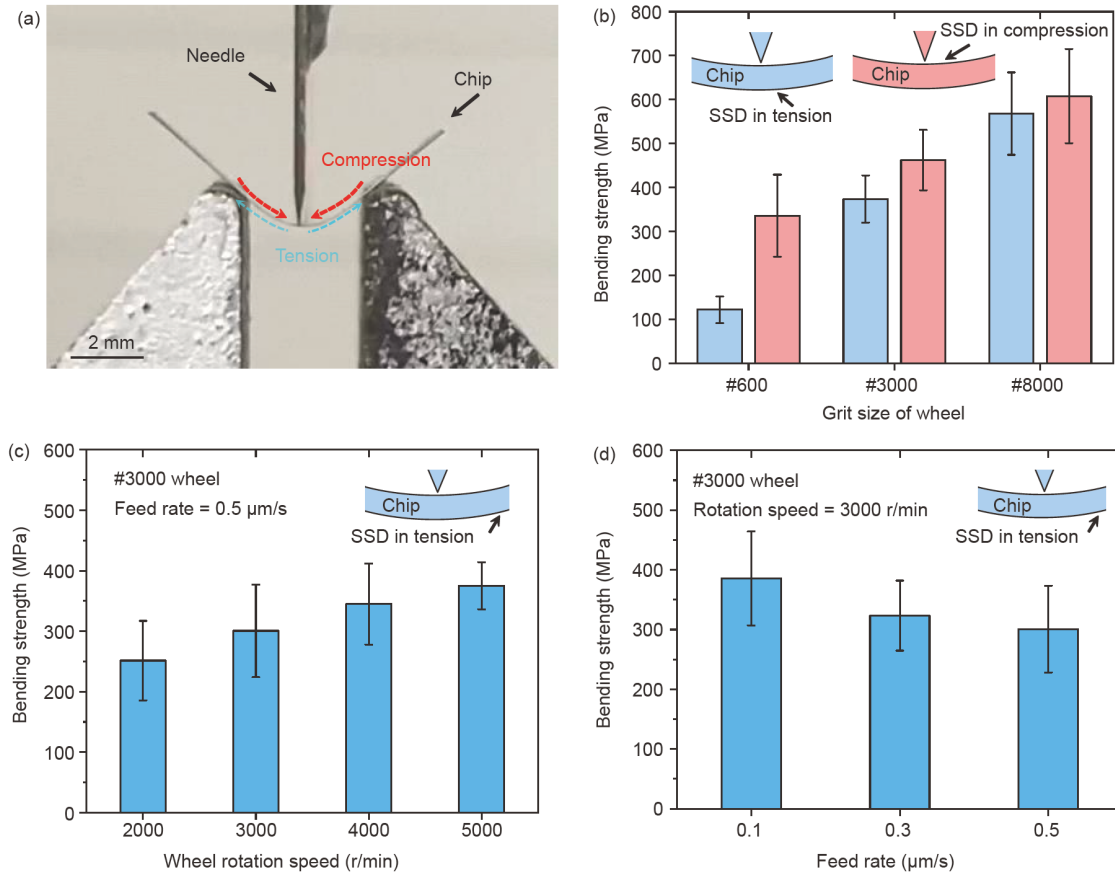


Figure 5 (a) Three-point bending test for the chip. Variation of bending strength with (b) grit size of the wheel, (c) wheel rotation speed, and (d) feed rate.

(#3000 wheel) and feed rate (0.5 μm/s), as shown in Figure 5(c). In the case of SSD in tension, the average bending strengths are 251, 301, 345, and 375 MPa for wheel rotations of 2000, 3000, 4000, and 5000 r/min, respectively. These results suggest that the bending strength becomes higher with increasing wheel rotation speed, which is attributed to the reduction in the SSD depth shown in Figure 3(c).

Similarly, the bending strength of ultra-thin chips processed under different feed rates with the same grit size (#3000 wheel) and wheel rotation speed (3000 r/min) is measured, as shown in Figure 5(d). Considering the situation where SSD is in tension, the average bending strengths are 385, 323, and 301 MPa for feed rates of 0.1, 0.3, and 0.5 μm/s, respectively. It is clear that bending strength decreases with increasing feed rate, which is consistent with the results in Figure 4(c).

Based on the above discussion, it is suggested that the bending strength is dependent on the SSD depth, i.e., the deeper the SSD, the lower the bending strength. In brittle solids, pre-existing cracks or flaws are detrimental because they can act as stress concentrators and significantly weaken the strength of the material. Compared with a single crystal with a perfect lattice structure, SSD including amorphization

and dislocation are crystal defects, which are the origin of local stress concentration during mechanical loading. Therefore, less stress concentration can be achieved by reducing the SSD depth. From the perspective of fracture mechanics, if the SSD depth δ is considered as the size of a pre-existing crack, the critical stress intensity at fracture can be determined using the following expression: $K_{IC} = Y\sigma\sqrt{\pi\delta}$, in which K_{IC} is the fracture toughness, Y is the geometrical factor depending on the damage location and sample shape, and σ is the applied stress at fracture. When the applied stress intensity factor reaches the critical value, the crack propagates and a fracture occurs. In general, the fracture toughness is a constant for a given material, hence, the applied stress at fracture (i.e., the bending strength) is inversely proportional to the SSD depth. In other words, when the SSD is deeper, a fracture will occur at a lower applied stress level. This explains why ultra-thin chips with deeper amorphization and dislocation exhibit lower bending strengths.

In addition, considering SSD may play a more important role in the degradation of bending strength when the thickness decreases down to several microns, the effect of chip thickness on the bending strength of ultra-thin chips with SSD is discussed, as shown in Figure S5. It is clear that bending strength decreases with increasing feed rate for

chips with thicknesses of both 20 and 100 μm . In addition, the bending strength of a 100- μm chip is higher than that of a 20- μm chip. This phenomenon can be explained as follows: On the one hand, for brittle solids, the maximum tensile stress criterion considers when the maximum tensile stress reaches the critical value, a crack propagates, and a fracture occurs. Based on the beam theory, the maximum stress occurs at the outermost part of the ultra-thin chip, which is provided by $\sigma_{\max} = \frac{Mh}{2I_z} = \frac{6M}{bh^2}$, where M is the bending moment, and I_z is the cross-sectional moment of inertia. Therefore, for a given external load, thinner chips are subjected to a higher level of stress and more likely to exceed critical stress. On the other hand, for a given process parameter, such as feed rate, the SSD depth is independent of the chip thickness. However, the defect volume fraction of thin chips is larger than that of thick chips, which results in more stress concentration and a higher probability of failure. Therefore, under the same process parameters, thinner chips exhibit lower bending strengths.

3.4 Bending strength after the removal of SSD

Based on the above discussion, it is expected that the bending strength is able to be improved by eliminating the stress concentrators. To remove the SSD induced by the grinding process, wet etching and chemical mechanical polishing (CMP) are applied respectively for 30- μm ultra-thin chips that are processed by #3000 wheel. In the wet etching process, the chip is exposed to HF/HNO₃ solution and etched for approximately 2 μm . Figure 6(a) shows the cross-sectional TEM image after etching (the region above the demarcation line is a deposited Pt layer to protect the sample during FIB, the region below the line is single crystal Si), and no crystal defects are observed, as shown in the inset HR-TEM image. This indicates that the SSD induced by grinding has been removed. However, the surface grooves induced by grinding cannot be completely removed by wet etching (Figure S4), resulting in a rough surface profile. CMP is used to create a damage-free structure through the cooperative processes of

mechanical removal and chemical corrosion. Figure 6(b) shows a TEM image after CMP processing. Obviously, there is a perfect lattice structure under the smooth surface, as shown in the inset HR-TEM image.

Compared with mechanical grinding, the results in Figure 6(c) show that wet etching and CMP can improve the bending strength by approximately 86% and 135%, respectively. These results prove that the removal of material defects can indeed improve bending strength, which is similar to the results of previous studies [9,38]. In other words, because the SSD depth is reduced, the applied stress intensity factor reaches the critical value and fracture occurs at a higher applied stress level. In addition, an imperfect surface profile will cause local stress concentration, therefore, CMP is more effective in improving bending strength than wet etching. In practical applications, the rough surface profile is beneficial to improve the bonding between the electrode and the backside of the chip. This implies that wet etching is suitable for improving the bending strength of chips with back electrodes, while CMP is more suitable for chips without back electrodes.

4 Conclusion

In summary, the relationship between SSD and the bending strength of chips under different grinding parameters is studied in this paper. SSD including amorphization and dislocation is observed by TEM. The variation of the SSD depth with different processing parameters is predicted theoretically and validated by experimental data. When the grit size or feed rate decreases, or wheel rotation speed increases, the depth of SSD decreases. The existence of SSD will cause stress concentration and degradation of bending strength. Moreover, there is a size effect of SSD depth on bending strength, that is, the deeper SSD becomes, the lower the chip bending strength will be. Therefore, optimizing grinding parameters can effectively result in the reduction of SSD depth, which will enhance the bending strength. The bending strength can be further enhanced after wet etching and chemical mechanical polishing (CMP), owing to the removal of

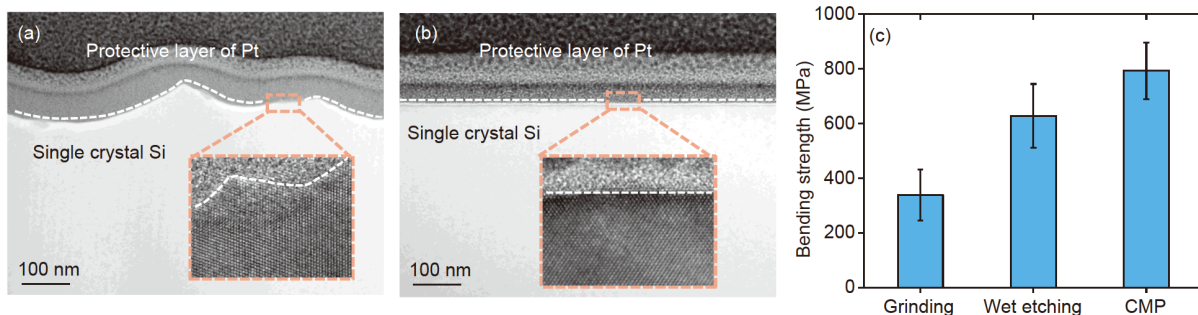


Figure 6 Representative TEM image of the subsurface after (a) wet etching and (b) CMP. Insets show HR-TEM images near the surface. (c) Variation of bending strength after grinding, wet etching, and CMP.

SSD. This study provides key information that can be used in the development and large-scale production of ultra-thin and flexible chips.

This work was supported by the National Natural Science Foundation of China (Grant Nos. U20A6001, 11625207, 11902292, and 11921002), and the Zhejiang Province Key Research and Development Project (Grant Nos. 2019C05002, 2020C05004, and 2021C01183).

Supporting Information

The supporting information is available online at tech.scichina.com and link.springer.com. The supporting materials are published as submitted, without typesetting or editing. The responsibility for scientific accuracy and content remains entirely with the authors.

- 1 Chen Y, Liu F, Lu B, et al. Skin-like hybrid integrated circuits conformal to face for continuous respiratory monitoring. *Adv Electron Mater*, 2020, 6: 2000145
- 2 Chen Y, Zhang Y, Liang Z, et al. Flexible inorganic bioelectronics. *Npj Flex Electron*, 2020, 4: 1
- 3 Jin P, Fu J, Wang F, et al. A flexible, stretchable system for simultaneous acoustic energy transfer and communication. *Sci Adv*, 2021, 7: 2507
- 4 Burghartz J N, Appel W, Harendt C, et al. Ultra-thin chip technology and applications, a new paradigm in silicon technology. *Solid-State Electron*, 2010, 54: 818–829
- 5 Gupta S, Navaraj W T, Lorenzelli L, et al. Ultra-thin chips for high-performance flexible electronics. *npj Flex Electron*, 2018, 2: 8
- 6 Ma Y, Zhang Y, Cai S, et al. Flexible hybrid electronics for digital healthcare. *Adv Mater*, 2020, 32: 1902062
- 7 Vandeperre L J, Giuliani F, Lloyd S J, et al. The hardness of silicon and germanium. *Acta Mater*, 2007, 55: 6307–6315
- 8 Wortman J J, Evans R A. Young's modulus, shear modulus, and Poisson's ratio in silicon and germanium. *J Appl Phys*, 1965, 36: 153–156
- 9 Yamaguchi H, Tatami J, Yahagi T, et al. Dislocation-controlled microscopic mechanical phenomena in single crystal silicon under bending stress at room temperature. *J Mater Sci*, 2020, 55: 7359–7372
- 10 Qin F, Zhang L, Chen P, et al. *In situ* wireless measurement of grinding force in silicon wafer self-rotating grinding process. *Mech Syst Signal Process*, 2021, 154: 107550
- 11 Delmdahl R, Pätzl R, Brune J. Large-area laser-lift-off processing in microelectronics. *Phys Procedia*, 2013, 41: 241–248
- 12 Wang C, Linghu C, Nie S, et al. Programmable and scalable transfer printing with high reliability and efficiency for flexible inorganic electronics. *Sci Adv*, 2020, 6: 2393
- 13 Sevilla G A T, Inayat S B, Rojas J P, et al. Flexible and semi-transparent thermoelectric energy harvesters from low cost bulk silicon (100). *Small*, 2013, 9: 3916–3921
- 14 Burghartz J N. Silicon-on-insulator (SOI) wafer-based thin-chip fabrication. In: Burghartz J, ed. *Ultra-thin Chip Technology and Applications*. New York: Springer, 2011. 61–67
- 15 Burghartz J N. You can't be too thin or too flexible. *IEEE Spectr*, 2013, 50: 38–61
- 16 Du D, Wu Y, Zhao Y, et al. Deformation and fracture behaviours of a YAG single crystal characterized using nanoindentation method. *Mater Charact*, 2020, 164: 110302
- 17 Huang H, Li X, Mu D, et al. Science and art of ductile grinding of brittle solids. *Int J Machine Tools Manuf*, 2021, 161: 103675
- 18 Lawn B R, Borrero-Lopez O, Huang H, et al. Micromechanics of machining and wear in hard and brittle materials. *J Am Ceram Soc*, 2021, 104: 5–22
- 19 Li C, Wu Y, Li X, et al. Deformation characteristics and surface generation modelling of crack-free grinding of GGG single crystals. *J Mater Process Tech*, 2020, 279: 116577
- 20 Zhou P, Yan Y, Huang N, et al. Residual stress distribution in silicon wafers machined by rotational grinding. *J Manuf Sci Eng*, 2017, 139: 081012
- 21 Gao S, Dong Z, Kang R, et al. Warping of silicon wafers subjected to back-grinding process. *Precis Eng*, 2015, 40: 87–93
- 22 Marshall D B, Lawn B R, Evans A G. Elastic/plastic indentation damage in ceramics: The lateral crack system. *J Am Ceramic Soc*, 1982, 65: 561–566
- 23 Wu C, Li B, Liu Y, et al. Strain rate-sensitive analysis for grinding damage of brittle materials. *Int J Adv Manuf Technol*, 2016, 89: 2221–2229
- 24 Yao Z, Gu W, Li K. Relationship between surface roughness and subsurface crack depth during grinding of optical glass BK7. *J Mater Process Tech*, 2012, 212: 969–976
- 25 Yin J, Bai Q, Goel S, et al. An analytical model to predict the depth of sub-surface damage for grinding of brittle materials. *CIRP J Manuf Sci Tech*, 2021, 33: 454–464
- 26 Zhang L, Chen P, An T, et al. Analytical prediction for depth of subsurface damage in silicon wafer due to self-rotating grinding process. *Curr Appl Phys*, 2019, 19: 570–581
- 27 Fang X, Bishara H, Ding K, et al. Nanoindentation pop-in in oxides at room temperature: Dislocation activation or crack formation? *J Am Ceram Soc*, 2021, 104: 4728–4741
- 28 Zhao J H, Tellkamp J, Gupta V, et al. Experimental evaluations of the strength of silicon die by 3-point-bend versus ball-on-ring tests. *IEEE Trans Electron Packag Manuf*, 2009, 32: 248–255
- 29 Liu Z, Huang Y A, Xiao L, et al. Nonlinear characteristics in fracture strength test of ultrathin silicon die. *Semicond Sci Technol*, 2015, 30: 045005
- 30 Jeon E B, Park J D, Song J H, et al. Bi-axial fracture strength characteristic of an ultra-thin flash memory chip. *J Micromech Microeng*, 2012, 22: 105014
- 31 McLellan N, Fan N, Liu S, et al. Effects of wafer thinning condition on the roughness, morphology and fracture strength of silicon die. *J Electron Packag*, 2004, 126: 110–114
- 32 Liu T, Ge P, Bi W, et al. Fracture strength of silicon wafers sawn by fixed diamond wire saw. *Sol Energy*, 2017, 157: 427–433
- 33 Wu J D, Huang C Y, Liao C C. Fracture strength characterization and failure analysis of silicon dies. *Microelectron Reliab*, 2003, 43: 269–277
- 34 Yang C, Mess F, Skenes K, et al. On the residual stress and fracture strength of crystalline silicon wafers. *Appl Phys Lett*, 2013, 102: 021909
- 35 Sun J, Qin F, Chen P, et al. A predictive model of grinding force in silicon wafer self-rotating grinding. *Int J Mach Tools Manuf*, 2016, 109: 74–86
- 36 Jing X, Maiti S, Subhash G. A new analytical model for estimation of scratch-induced damage in brittle solids. *J Am Ceram Soc*, 2007, 90: 885–892
- 37 Hu J Z, Merkle L D, Menoni C S, et al. Crystal data for high-pressure phases of silicon. *Phys Rev B*, 1986, 34: 4679–4684
- 38 Uchic M D, Dimiduk D M, Florando J N, et al. Sample dimensions influence strength and crystal plasticity. *Science*, 2004, 305: 986–989